ELSEVIER

Dynamics of Atmospheres and Oceans 24 (1996) 51–62

dynamics of atmospheres and oceans

Convection, entrainment and mixing

Turbulent mixing in the oceanic boundary layer caused by internal wave reflection from sloping terrain

Donald N. Slinn, James J. Riley *

University of Washington, Department of Mechanical Engineering, 256 Mechanical Engineering Building, Seattle, WA 98195, USA

Received 1 July 1994; revised 28 February 1995; accepted 6 March 1995

Abstract

Strong diapycnal mixing may occur in the benthic boundary layer caused by internal wave breakdown into turbulence near sloping boundaries. We report on numerical simulations of internal wave reflection and mixing in the bottom boundary layer over sloping topography. The experiments presented here are for critical angle wave reflection, defined as reflection from a bottom slope which matches the wave propagation angle. We demonstrate that transition of the wave field to stratified turbulence occurs for Reynolds number of approximately 1000. The turbulent boundary layer, of approximate thickness $\lambda/3$, where λ is the wavelength of the oncoming wave, exhibits quasi-periodic behavior, going through a cycle of energetic mixing and fine-scale development followed by a period of restratification and relaminarization. A distinctive thermal front develops in the boundary layer, which moves upslope at the phase speed of the oncoming wave. For steep slopes the flow resembles a turbulent bore, whereas for shallower slopes periodic mixing occurs across the breadth of the domain. The strongest period of mixing occurs during a phase when the oncoming wave sets up a strong downslope flow at the bottom boundary similar to the backwash on a beach. We find that diapycnal mixing extends into the interior stratified fluid and is not restricted to the turbulent boundary region. An important element of the communication of mixed fluid into the interior is the action of the internal wave field. It serves to continuously pump fresh stratified fluid into the mixed layer, while simultaneously extracting the mixed boundary fluid. The mixing efficiency of the wave breakdown process for these cases is found to be approximately 35%.

1. Introduction

Gaining an improved understanding of vertical mixing in the ocean is an important problem in physical oceanography. Large-scale dynamic models require

* Corresponding author.

SSDI 0377-0265(95)00425-4

accurate parameterizations for turbulent mixing to make realistic predictions for the transport of heat, salt, and chemical species. Other important processes also involve vertical mixing. For example, vertical mixing supplies the biological ecosystem with necessary ingredients, as heavy, nutrient-rich bottom water is lifted to the surface to support plant and animal life. The ocean is stably stratified, which acts to inhibit vertical mixing. Munk (1966) has shown that a basin-averaged vertical eddy diffusivity of roughly $\kappa = 10^{-4}$ m^2 s^{-1} must exist to balance the effects of upwelling and downward diffusion. Field studies, however, have failed to observe such large vertical diffusivities in the ocean interior. Typical measured values for vertical diffusivity in the open ocean are approximately $\kappa = 1.2 \times 10^{-5}$ m^2 s^{-1} (Ledwell et al., 1993). The conclusion from the experiments is that 80–90% of the vertical mixing is not taking place in the ocean interior.

Instead, the mixing is expected to occur at the boundaries, near continental slopes, islands, seamounts, and other topographic features. The idealized picture is one of active mixing in the benthic boundary layers with mixed fluid communicated to the interior along constant density surfaces. The exchange of mixed boundary fluid with interior stratified fluid provides a mechanism to weaken the interior density gradient, and continuously supply fresh stratified fluid to be mixed in the boundary layer. The overall process can work efficiently as horizontal advection is not inhibited by the surrounding stratification. Recent field experiments (Eriksen, 1985, 1995) have suggested that the oceanic internal wave field can provide a sufficient source of energy to activate strong mixing near sloping boundaries and account for a significant portion of the overall oceanic vertical mixing.

The angle of propagation of energy of an internal wave depends upon the wave frequency, ω, and the background density stratification according to the dispersion relation $\omega = N \sin \theta$, where N is the buoyancy frequency defined by $N^2 = (-g/\rho_0)(\partial\rho/\partial z)$, and θ is the angle between the group velocity vector and the horizontal. When an internal wave reflects from a larger-scale sloping boundary, its angle of propagation with respect to the horizontal is preserved. This can lead to an increase in the energy density of the reflected wave, as illustrated in Fig. 1 for a linear internal wave ray tube. The energy in the oncoming wave is concentrated into a more narrow ray tube upon reflection, and the magnitude of its group velocity is decreased.

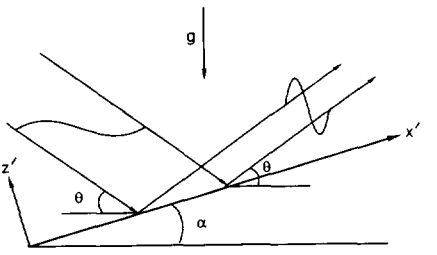

Fig. 1. Ray tube diagram of internal gravity wave reflection from sloping terrain illustrating the basic geometry of the problem.

Probably the most effective situation for boundary mixing arises when an oncoming wave reflects from a bottom slope which nearly matches the angle of wave propagation. In this case, a small-amplitude oncoming wave may be reflected with large amplitude and exhibit nonlinear behavior. The nonlinearity can cause the wave to undergo a transition to turbulence near the boundary and enhance mixing of the boundary layer fluid. The angle of wave propagation such that the wave reflects at the same angle as the bottom slope is called the critical angle. In this case, linear wave theory predicts a reflected wave of infinite amplitude and infinitesimal wavelength and the trapping of the oncoming wave energy in the boundary region. In such a case, linear theory is clearly inadequate to predict the flow behavior, as nonlinearities and turbulence come into play.

In this paper we present the results of numerical experiments simulating the reflection of internal wave trains from bottom terrain of various slopes. The numerical experiments complement previous field and laboratory studies (Ivey and Nokes, 1989; Taylor, 1993) with the ability to study the energetics and turbulence dynamics in detail. Additional strengths of the numerical approach include facilitating both flow visualization and parameter studies on the influence of key physical and nondimensional quantities. It offers the ability to simulate critical angle reflection down to slopes of about 3°, which are typical of oceanic conditions (Thorpe, 1992).

2. Model description

The model utilizes state-of-the-art numerical techniques to solve the three-dimensional, incompressible Navier–Stokes equations within the Boussinesq approximation. A detailed description of the physical and numerical model is to appear in a separate paper (Slinn and Riley, 1995). The problem of interest is to simulate the reflection of internal waves from the ocean floor. The buoyancy frequency N is taken to be constant, and a steady stream of oncoming waves is generated in a wave forcing region located away from the ocean floor. This is accomplished by adding localized forcing terms to the governing equations to produce a monochromatic train of waves with a specified wavelength and frequency. The waves propagate downward at a specified angle θ with respect to the horizontal, with group velocity $\boldsymbol{C}_g$, and wavenumber $\mathbf{k} = (k, l, m)$.

Fig. 2 shows isopycnals taken at an intermediate time from a numerical experiment in which the internal wave train is propagating in a vertical plane (x', z') normal to the terrain surface. It represents a two-dimensional cross-section of the density field of a three-dimensional simulation taken in the plane of the slope. The constant density contours indicate the amplitude of the oncoming wavetrain as well as show the development of a region of strong density gradient near the bottom boundary. The oncoming waves are of moderate amplitude and approach the wall in the plane of the slope. Here the bottom slope is 9.2° and the fundamental frequency of the oncoming wave is chosen so that the propagation angle matches the bottom slope upon reflection, e.g. the wave is at the critical

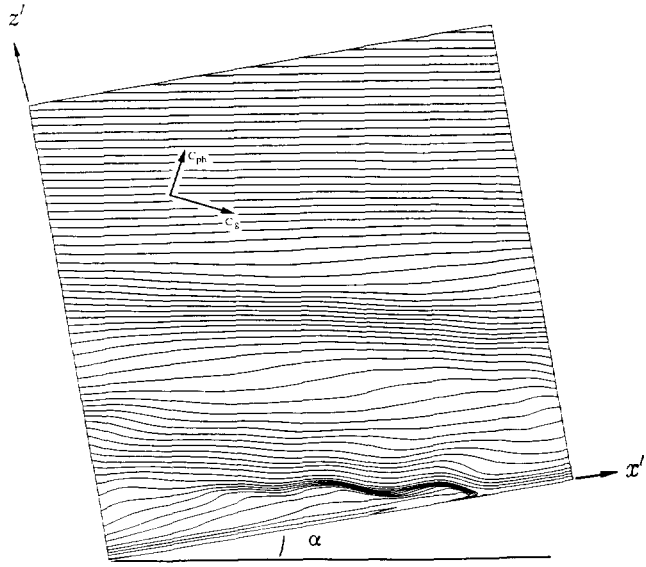

Fig. 2. Density contours for an oncoming wave train generated in a forcing region above the bottom boundary propagating downward with phase and group velocities as indicated.

angle. For the geometry of Figs. 2–4 $\lambda_x = 3\lambda_z$, where λ_x and λ_z refer to the wavelengths in the x' and z' directions. The aspect ratios, $x' : z'$, are shown to scale in Figs. 2, 3 and 5–7. For this case, the actual wavelength is $\lambda = 0.95\lambda_z$ according to the relation $1/\lambda^2 = 1/\lambda_x^2 + 1/\lambda_z^2$.

The model is taken to be periodic in the y direction with the width of the domain in the y direction, y_l, set comparable with λ_x and λ_z; in this case, $y_l = 1.7\lambda_z$. The model is made periodic in the x' (upslope) direction by subtracting the background (linear) density stratification from the governing equations and formulating conservation equations for perturbation density and pressure fields about the mean resting state. It is possible to reformulate the problem in this manner for constant N as the background density stratification is in hydrostatic balance with the pressure field. The bottom boundary conditions are no-slip for the velocity field and adiabatic (no flux of heat or salt) for the density field.

The numerical scheme employs the pressure projection method, implemented with a variable time step third-order Adams–Bashforth scheme to achieve high temporal accuracy. Padé series expansions are used as the basis functions for spatial discretization. The method is formally fourth-order accurate in space and more accurately represents a wide range of wavenumbers than traditional difference schemes (Adam, 1977; Lele, 1992). The pressure field is determined by solving a Poisson equation using Fourier transforms in the lateral directions and a fourth-order direct solution method in the vertical direction. A Rayleigh damping sponge layer is used at the top open boundary to mimic a radiation boundary condition. A variable grid in the vertical direction is used to achieve a higher

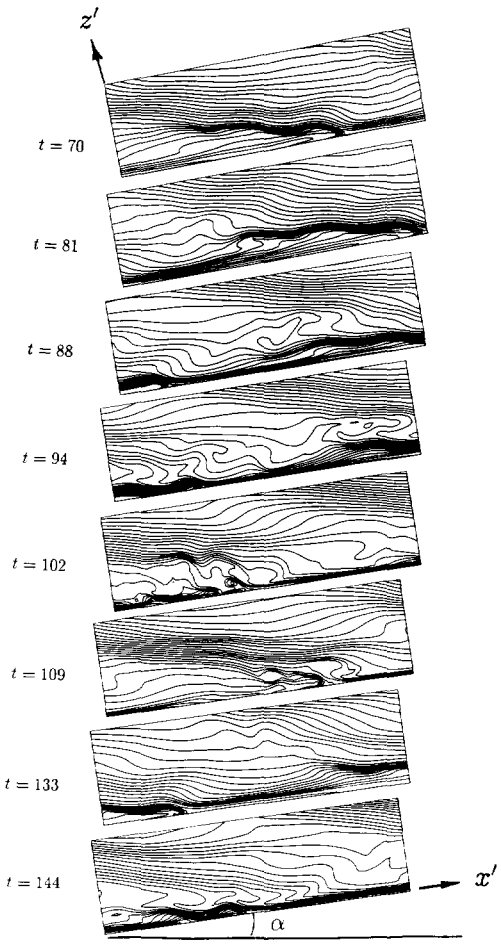

Fig. 3. Time series of flow development in the near-wall region.

density of computational nodes near the bottom boundary to resolve the boundary layer. The computations were carried out on a numerical grid using $129 \times 65 \times 130$ grid points. Care was taken so that the basic features of the flow are resolved throughout the simulations. The Reynolds numbers for the simulations, Re, based upon the current speed U and wavelength λ, are between 500 and 3500.

3. Results

Fig. 3 shows a time series, visualized by constant density surfaces, depicting the flow development throughout a period of wave breakdown. The figures focus on the near-wall region. The dimensions are one wavelength, $\lambda_z = 2\pi/m'$, in the z'

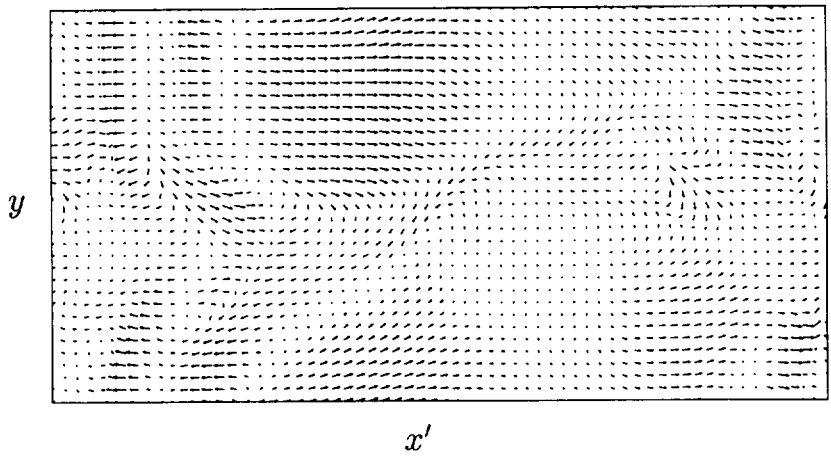

Fig. 4. Velocity vectors in a plane parallel to the wall located within the boundary layer at $t = 94$.

direction by one wavelength, $\lambda_x = 2\pi/k'$, in x' direction. The figures are taken from a simulation with Re = 3500 for the critical angle case with a bottom slope of 9.2°, the same case as shown in Fig. 2. Here time is nondimensionalized by the buoyancy frequency and the wave period is 39.2. At time $t = 70$ the wave train has reached the wall and a steep gradient in density has formed. This feature, called a thermal front by Thorpe (1992), moves upslope at the x' component of the phase speed of the oncoming wave. As time progresses, wave overturning develops in the lee of the thermal front, and at time $t = 88$, statically unstable fluid is apparent near the center of the domain. Another significant feature is also apparent at times $t = 88$ and $t = 94$. Near the wall, a region of steep density gradient has developed in the z' direction and across the entire breadth of the domain. As time continues, the overturned regions break down into small-scale turbulence and dissipate the wave energy in a three-dimensional fashion. Also, the steep density gradient in the z' direction is relieved, so that by $t = 109$ it is no longer a dominant feature of the flow.

Fig. 4 indicates some of the three-dimensional structure of the flow during the wave breakdown phase. It shows vectors of the u'–v velocity components in an x'–y plane parallel to the bottom slope at a distance from the wall of $z' = 0.126\lambda_z$. The vectors appear to represent a divergent flow because they show only the components of velocity in the x'–y plane and do not include the w' component. The velocity field is taken at $t = 94$, and the dimensions of the x' and y directions are $3\lambda_z$ and $1.7\lambda_z$, respectively. Several distinct horizontal structures are apparent in the flow, including jets and fronts associated with the unstable density profiles. The observed variability in the y direction is an indication of the importance of using a 3-D model to capture the physics of the wave breakdown process.

Further analysis of the velocity fields, not pictured here, indicates several small eddies of circulating fluid actively participating in vertical mixing. The eddies are

associated with the regions of overturned fluid and are three-dimensional in character. When the strong density gradient in the z' direction occurs, a strong region of downslope flow is produced near the wall, similar to the backwash produced on a beach after a wave has broken on shore. During this phase the backwash creates a slippery boundary layer, facilitating the breakdown of the oncoming wave further away from the wall.

Further analysis indicates that the flow is quasi-periodic, going through a cycle of strong mixing and small-scale dissipation, followed by a quieter period of relaminarization and weaker dissipation. The picture at time $t = 133$ is similar in character to the flow at about $t = 81$, and $t = 144$ compares closely with the picture at $t = 94$, showing that the flow is undergoing another mixing cycle. Some of the simulations have been run for 10–20 wave cycles, and we conclude that the flows are quasi-steady, although the background interior density stratification becomes gradually weakened throughout the process. Statistical analysis of the overturned regions of fluid indicate that the static instabilities mainly occur within a distance of $\lambda_z/3$ of the wall, and are present in the boundary layer region about 50% of the time. This result is typical of critical angle cases for many different slopes when the Reynolds numbers are high enough for transition to turbulence to occur. Another measure of the local static instabilities is their frequency of occurrence at a fixed location. For a fixed location within the turbulent boundary layer, the maximum frequency of static instability is about 15% of the time, and it happens at a height of about $\lambda_z/8$.

A key issue related to the wave breakdown process is whether the turbulent boundary layer exchanges fluid with the interior domain or whether it predominantly continues to mix the same fluid. Two experiments were designed to study this issue. In the first, the boundary layer fluid is 'dyed' with a passive tracer after the flow has reached a quasi-steady state of mixing. Then after a couple of wave periods the flow is examined to determine if the dye is still predominantly located in the boundary layer region, or if it has moved off the wall to the interior stratified regions. For the case presented here, a scalar field with an initial linear gradient in the z' (off-wall) direction was chosen and allowed to develop for two wave periods. The initial concentration, or magnitude of the scalar field, is highest at the wall, its value falling off with height. Any net transport of dye owing to the waveshear is approximately eliminated by examining the results after an integral number of wave periods. The second approach is to track fluid particles which are released at various heights, and to determine if a statistically significant number of particles escape from the boundary mixed layer, or if particles initially outside the boundary layer are entrained into it.

Figs. 5–7 illustrate the results of these experiments. Fig. 5 shows a 2-D cross-section of the density field for the lowest vertical wavelength for critical angle reflection over a 20° bottom slope. The dimensions for this case are $\lambda_x = 1.2\lambda_z = y_l = 1.56\lambda$. The figures could be tilted 20° upslope to be in their natural frame of reference but are more naturally compared side by side. The density field indicates that the mixed layer has a thickness of about $0.25\lambda_z$. These figures are taken at a time when the flow field is quasi-steady, and are representative of the initial and

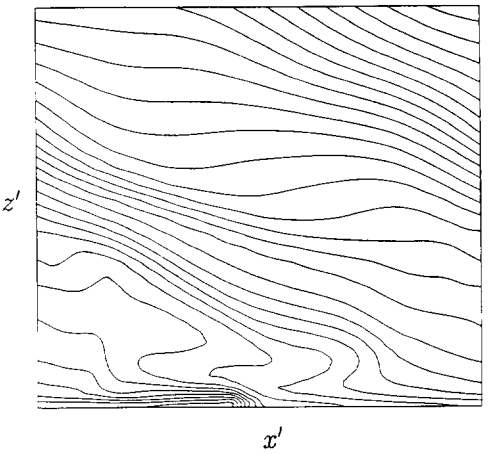

Fig. 5. Density field at the end of the dye experiment.

final states of the flow for the dye experiment. Fig. 6 illustrates the velocity vectors in the same two-dimensional plane. Here the dominant feature is the shear of the oncoming wave, modified somewhat by recirculation and turbulence in the near-wall regions. Fig. 7 shows the difference in concentration of the scalar field between its initial and final states. The continuous line contours indicate that the concentration of dye (scalar) is higher than in the initial state, indicating that fluid has migrated away from the wall in those regions. The dashed line contours indicate

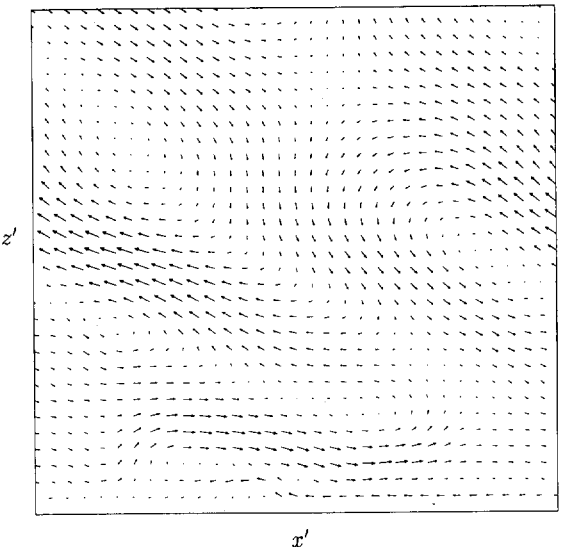

Fig. 6. Velocity field at the end of the dye experiment.

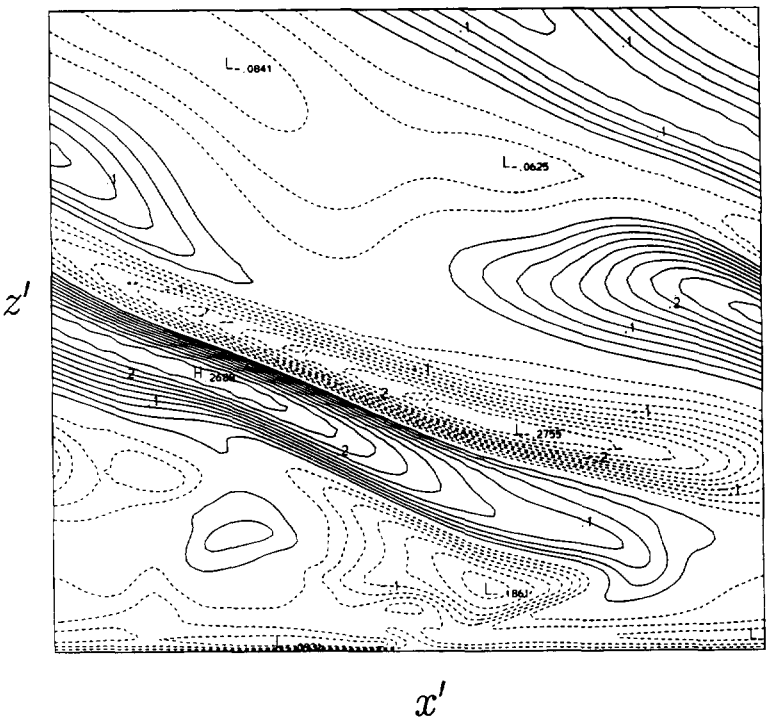

Fig. 7. Scalar transport contours illustrating the distance dyed fluid has traveled in the off-wall direction over the duration of two wave periods.

regions in which more dilute or lighter dyed fluid has moved toward the wall. It is evident that the boundary layer region contains predominantly lighter dyed fluid after two wave periods. The magnitudes of the highs and lows indicate the fraction of a wavelength in the vertical (off-wall) direction that the scalar tracer has moved. For example, the high and low peaks at a height of about $0.4\lambda_z$ are 0.268 and -0.275, respectively. This indicates that the fluid has traveled over $0.25\lambda_z$ in the off-wall direction, a distance greater than the nominal boundary layer thickness. By comparing the slope of the scalar transport contours with the slope of the isopycnals in Fig. 5 it is evident that the advection process has favored transport along the constant density surfaces as the iso-scalar-transport and isopycnals are predominantly aligned with one another.

A significant feature of the boundary mixing process is that the internal wave field outside the boundary layer region plays a very active role. It serves to continuously pump fresh stratified fluid into the mixed layer, while simultaneously extracting the mixed fluid. This process is suggested by the strong internal wave shear seen in the velocity field in Fig. 6. We refer to this exchange of boundary mixed and stratified fluid as internal wave pumping.

Fig. 8 shows the traces in the x–z plane of the three-dimensional trajectories of a set of 20 (out of a total of 400) fluid particles released at a height of $0.2\lambda_z$ from

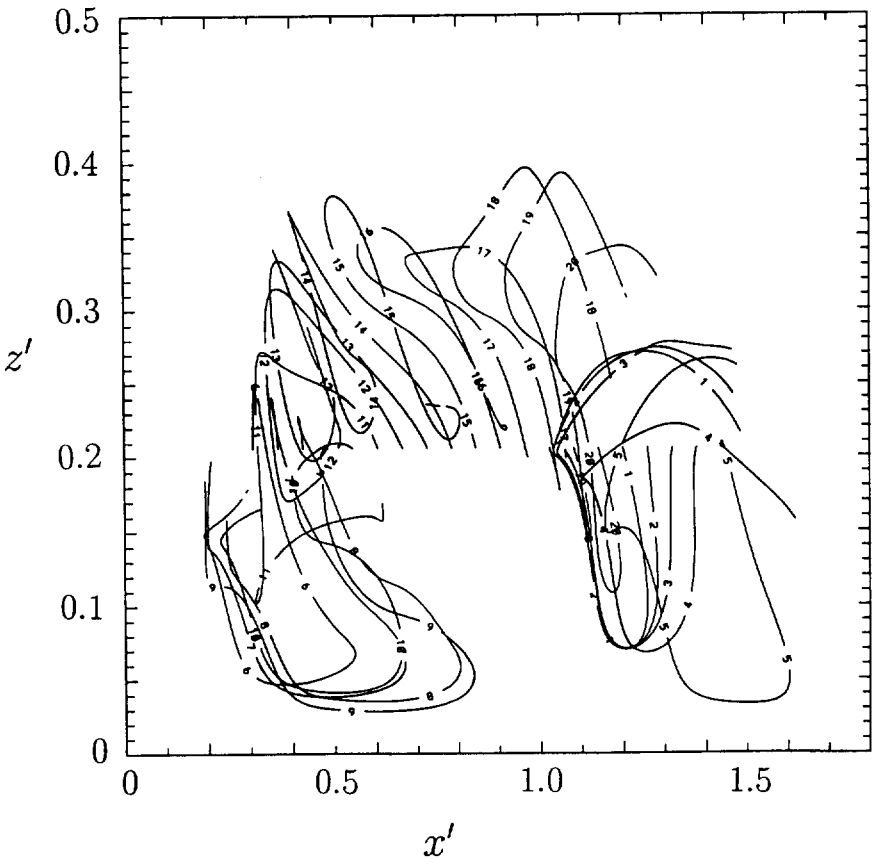

Fig. 8. Particle trajectories over one wave period. The fluid particles were initially released at a height of $0.20\lambda_z$ within the turbulent boundary layer.

the wall, well within the mixed layer. The dimensions of Fig. 8 are $0.5\lambda_z$ in the z' direction and $1.8\lambda_x$ in the x' direction. The x' axis is periodic after the point $1.0\lambda_x$ but has been expanded for this figure so that the particle trajectories do not seem to jump from one boundary to another. The particles are followed for one wave period. If the particles were released in a region of linear wave dynamics, in a monochromatic wave field, then, after one wave period, they would return to their initial locations. Here we see that several of the particles have escaped the boundary layer altogether, and many others have been more deeply entrained near the wall. After each additional wave period the particle dispersion has increased and appears to be more random.

In the analysis of the simulations, emphasis is given to the energetics of the flows. Table 1 presents the mixing efficiency for a series of simulations for a number of different critical slopes. The mixing efficiency is defined as the ratio of the total potential energy dissipation to the total work used to generate the

Table 1
Mixing efficiency at critical angle

Slope (deg)	Reynolds no.	Mixing efficiency
30	3000	0.37
30	800	0.37
20	1800	0.36
20	1100	0.35
9.2	3540	0.35
9.2	2680	0.37
9.2	1950	0.36
9.2	1210	0.38
7.7	3000	0.35
7.7	1500	0.33
7.7	750	0.37
5	3300	0.37
5	2300	0.39
5	1800	0.38
3.4	2520	0.37
3.4	1320	0.35

oncoming wave train, and is a measure of the amount of wave energy converted into background potential energy through mixing. We find, for these critical angle simulations carried out for a wide range of bottom slopes and Reynolds numbers, that all the mixing efficiencies are near 35%. It is suspected that these high values for mixing efficiencies may be Reynolds number dependent. The moderately low Reynolds numbers of the numerical experiments, together with a Prandtl number of unity, drive the mixing efficiencies toward a value of 50%. These results do not contradict the laboratory measurements of mixing efficiency by Ivey and Nokes (1989) and Taylor (1993) of approximately 20% which were conducted in a higher regime of Reynolds, Richardson, and Prandtl numbers. A typical energy budget for the oncoming waves in the numerical experiments is that about 35% of the wave energy goes into mixing the stratified fluid, 55% is dissipated as heat, and approximately 10% of the incident energy is reradiated away from the turbulent boundary layer by smaller-scale gravity waves.

4. Conclusions

We have shown some of the details of a fluid mechanical process, involving the frequent breaking of internal waves near sloping ocean boundaries, which probably makes a large contribution to the vertical mixing in the ocean. We find that freely propagating oncoming gravity waves undergo a transition to turbulence when reflecting from a critical slope, and that the mixing efficiency of the process is about 35%. For steeper sloping terrain the transition Reynolds numbers, based upon wave current speed and wavelength, for which vigorous three-dimensional mixing occurs in the boundary layers, are approximately 1000. Somewhat higher

Reynolds numbers are required for transition for the more shallow slopes. We find also that an intermittent turbulent boundary layer forms, of approximate thickness $\lambda/3$, in which static instabilities are observed about 50% of the time.

One of the flow features most strongly evident is the existence of a thermal front which moves upslope at the phase speed of the oncoming wave. For steep slopes (greater than 20°) the thermal front resembles a turbulent bore exhibiting nearly continuous localized mixing, whereas for shallower slopes (less than 10°) the mixing is observed across the breadth of the domain and is temporally periodic. For the small slopes the turbulence is forced by the oncoming waves and the cycles of strong mixing and dissipation are approximately equal to the wave period. The strong mixing occurs during the phase when the oncoming wave sets up a strong downslope flow at the bottom boundary, similar to the backwash on a beach.

We find that the mixing process extends into the interior stratified fluid and is not restricted to a well-mixed boundary region. A key process in this interior communication is the internal wave pumping of mixed fluid into the interior and stratified fluid into the boundary layer. A net result of this process is a steady weakening of the interior stratification. Our results confirm those from field and laboratory studies that conclude that wave reflection from critically sloping terrain is a significant sink for internal wave energy.

Acknowledgments

This study was supported under US Navy Office of Naval Research Contract N00014-90-J-1112. The simulations were conducted on the Cray-2 and Cray YMP computers at the National Center for Supercomputer Applications.

References

Adam, Y., 1977. Highly accurate compact implicit methods and boundary conditions. J. Comput. Phys., 24: 10–22.

Eriksen, C.C., 1985. Implications of ocean bottom reflection for internal wave spectra and mixing. J. Phys. Oceanogr., 15(9): 1145–1156.

Eriksen, C.C., 1995. Internal wave reflection and mixing at Fieberling Guyot. J. Geophys. Res., submitted.

Ivey, G.N. and Nokes, R.I., 1989. Vertical mixing due to the breaking of critical internal waves on sloping boundaries. J. Fluid Mech., 204: 479–500.

Ledwell, J.R., Watson, A.J. and Law, C.S., 1993. Evidence for slow mixing across the pycnocline from an open-ocean tracer-release experiment. Nature, 364: 701–703.

Lele, S.K., 1992. Compact finite difference schemes with spectral like resolution. J. Comput. Phys., 103: 16–42.

Munk, W.H., 1966. Abyssal recipes. Deep-Sea Res., 13: 707–730.

Slinn, D.N. and Riley, J.J., 1995. A model for the simulation of a turbulent boundary layer in a stratified fluid, in preparation.

Taylor, J.R., 1993. Turbulence and mixing in the boundary layer generated by shoaling internal waves. Dyn. Atmos. Oceans, 19: 233–258.

Thorpe, S.A., 1992. Thermal fronts caused by internal gravity waves reflecting from a slope. J. Phys. Oceanogr., 22: 105–108.